energies

MDPI

Article

Analysis of Future Solar Power Potential Using CORDEX-CORE Ensemble in Côte d'Ivoire, West Africa

N'da Amoin Edith Julie Kouadio [1,*], Windmanagda Sawadogo [2], Aka Jacques Adon [3], Boko Aka [4], Yacouba Moumouni [5] and Saidou Madougou [6]

1 West African Science Service Centre on Climate Change and Adapted Land Use (WASCAL), University Abdou Moumouni of Niamey, Niamey P.O. Box 10662, Niger
2 Institute of Meteorology and Climate Research (IMK-IFU), Karlsruhe Institute of Technology (KIT), Campus Alpin, 82467 Garmisch-Partenkirchen, Germany; windmanagda.sawadogo@kit.edu
3 Equipe de la Physique pour l'Environnement, Laboratoire de Physique Fondamentale et Appliquée, Université Nangui Abrogoua, Abidjan 02 BP 801, Côte d'Ivoire; adonjacks1@gmail.com
4 Institut de Recherche sur les Energies Nouvelles (IREN), Université Nangui Abrogoua, Abidjan 02 BP 801, Côte d'Ivoire; bokom2010@gmail.com
5 Department of Electrical and Electronics Engineering, Higher Colleges of Technology, Ras Al Khaimah Women's Campus, Ras Al Khaimah P.O. Box 4792, United Arab Emirates; yakedz@gmail.com
6 Laboratory of Energetics, Electronics, Electrical Engineering, Automation and Industrial Computing (LAERT-LA2EI), University Abdou Moumouni of Niamey, Niamey P.O. Box 10963, Niger; nassara01@yahoo.fr
* Correspondence: kouadio.n@edu.wascal.org

Abstract

Renewable energy is an important pillar of decarbonization in reducing the impact of climate change. Among the renewable energy sources, solar photovoltaic energy is one of the fastest-growing across West Africa, especially in Côte d'Ivoire. However, its dependence on weather and climate could affect future power system operations. This study aims to quantify how climate change could affect future solar PV potential in Côte d'Ivoire under the RCP8.5 scenario. For this purpose, we used three regional climate model simulations (RCMs) generated by the new high-resolution Coordinated Regional Climate Downscaling Experiment (CORDEX) for the Africa domain (AFR-22). Future changes were computed for two time slices: the near future (2021–2040) and the middle future (2041–2060), relative to the reference period (1986–2005). The performance of the RCMs and their ensemble mean in simulating relevant climate variables was first evaluated with respect to the ERA5 reanalysis and satellite-based (SARAH-2) data during the reference period. Our results indicate that all available RCMs and their ensemble mean reasonably simulate the annual cycle and the spatial patterns features of surface solar radiation, near-air temperature and solar PV potential in Côte d'Ivoire. We also conclude that Côte d'Ivoire is expected to experience a moderate decrease in annual mean solar PV potential during the mid-21st century. The average decrease in solar PV potential over Côte d'Ivoire could range from 0.55% to 2.16% in the near future and from 1.30% to 3.50% during the middle future, according to the considered RCMs. This decline in solar PV potential will be particularly noticeable during the period from June to October in all climatic zones. Overall, these findings provide valuable information for renewable energy planners to ensure the long-term success of solar PV energy projects in the context of climate change in Côte d'Ivoire.

Keywords: climate change; solar photovoltaic potential; renewable energy; CORDEX-CORE; Côte d'Ivoire

Academic Editor: Massimo Dentice D'Accadia

Received: 26 January 2026
Revised: 11 March 2026
Accepted: 12 March 2026
Published: 24 March 2026

1. Introduction

Climate change is one of the world's foremost environmental challenges, affecting several sectors, such as water security, electricity systems, food security, and human well-being [1,2]. Climate change, however, has a negative impact on socio-economic development in many countries worldwide, particularly in West African countries, which are among the most vulnerable to climate change. According to the Intergovernmental Panel for Climate Change (IPCC) Fifth Assessment Report (AR5), the impact of climate change is expected to increase in the near and long-term future globally. In West Africa, climate change will strongly impact different sectors compared with other African regions [3]. The main driver of this phenomenon is the exponential increase in anthropogenic emissions of greenhouse gases, due principally to the energy sector through the burning of fossil fuels (such as coal, natural gas, and oil [4,5]. In 2024, the burning of fossil fuels contributed around 74.5% of global greenhouse gas emissions since 1990 [5].

Despite abundant renewable energy resources, power generation in West Africa remains dependent on fossil fuels. For instance, in Côte d'Ivoire, the electricity generation mix is composed of 76% gas thermal plants, 24% hydropower, and less than 1% solar energy [6,7]. Therefore, the growing demand for electricity, driven by economic and demographic growth, will lead to a continuous increase in greenhouse gas emissions unless drastic mitigation policies are implemented. Hence, the Earth's climate and regional climate can significantly change in the future [8].

To address the challenges of climate change, the first global climate agreement, called the Paris Agreement, was established by 195 countries in 2015. In fact, countries pledged to reduce their carbon emissions by making public their Nationally Determined Contributions (NDCs), with the aim of limiting the global average temperature to below 2 °C above preindustrial levels and pursing efforts to maintain it at 1.5 °C [9,10]. Indeed, around 99% of the communicated NDCs cover the energy sector [9,11]. Most of the NDCs promote the integration of low-carbon technologies and renewable energy as measures to reduce greenhouse gas emissions from the power sector [12]. In this regard, West African countries have taken action to mitigate climate change by adjusting their policies for electricity generation, with a focus on increasing the share of renewable energy in their electricity mix from 2020 to 2030 [13]. According to Abudu et al. [14], African countries have committed to reducing greenhouse gas emissions by 32% by 2030. In line with the objectives of the Paris Agreement, the government of Côte d'Ivoire has reviewed its energy policy and climate regulations to reduce its greenhouse gas emissions to 28.25–30.41% by 2030 [15]. This ambition implies the deployment of 42% renewable energy, such as hydropower, biomass, and solar power, in the electricity sector by 2030 [16–18].

Among renewable energy sources, solar photovoltaic energy technology is expected to rise significantly in the upcoming decades [19] due to its low operating cost, scalability, near-zero emissions during operation, improved efficiency, and increasingly competitive costs. The International Energy Agency has projected that the installed solar PV generation capacity will increase from 7 GW in 2020 to approximately 130 GW by 2030 under its Sustainable Africa Scenario [20]. For instance, many solar PV projects are currently installed or planned in Côte d'Ivoire, with a total capacity of 678 MW by 2030 and around 1686 MW by 2040 [21]. Moreover, the contribution of solar PV energy capacity, which is currently less than 1%, is expected to increase to 9% of the national electricity mix by 2030 in Côte d'Ivoire [22,23].

However, solar PV is highly influenced by local meteorological conditions, such as near-surface wind speed, solar irradiance, and near-surface temperature, snow, and dust [24,25]. Therefore, any changes in atmospheric conditions and climate change are

likely to significantly affect solar PV power [26–28] and also impact its integration into existing and future energy grids.

Accurate modeling is critical for maximizing the performance of solar PV systems, as they are sensitive to climate conditions. Recent research by Adar et al. [29] demonstrate that bond graph modeling combined with genetic algorithm optimization can produce highly accurate solar PV system models. This approach allows for precise estimation of key PV parameters, ensuring that system predictions remain reliable even under variable environmental conditions. Integrating such optimized models is particularly relevant in West Africa, where high temperatures and dust events can adversely affect solar PV efficiency, and adaptive modeling strategies are necessary to maintain energy output.

Regarding the sensitivity of solar PV energy to climate conditions, multiple studies have examined how climate change may affect solar PV power generation across different regions of Africa. They used the output of climate models from the Regional Climate Downscaling Experiment (CORDEX), the Coupled Model Intercomparison Project Phase 5 (CMIP5), and Phase 6 (CMIP6) under various climate scenarios. For example, Sawadogo et al. [30] employed the RegCM4 from the CORDEX-CORE ensemble to assess the impact of climate change on solar energy potential over Africa under low-end (RCP2.6) and high-end (RCP8.5) emission scenarios. Their results showed a general decrease in solar PV potential across the continent, except in some parts of Central Africa. On the other hand, some researchers [28,31,32] have revealed that solar PV power output is expected to decrease in most Africa countries based on CORDEX-AFRICA data. In addition, CORDEX-CORE simulations for Africa [33] and the Coupled Model Intercomparison Project Phase 6 (CMIP6) models [27] have been employed to evaluate the future evolution of solar power generation across West Africa. The authors concluded that solar PV potential is expected to generally decrease in West Africa under the worst-case climate scenario.

Moreover, these previous studies have clearly demonstrated that changes in solar irradiance and temperature induced by ongoing global warming can influence solar power potential, and the positive or negative impacts are likely to vary regionally. Some researchers revealed that intense cloudiness, higher temperatures, and dust observed in West Africa could negatively affect solar PV potential [27,34–36]. In Côte d'Ivoire, studies examining the impact of climate change on solar PV production are scarce in the literature.

The contribution of the present work is to evaluate the projected change in solar PV energy potential in Côte d'Ivoire under the high-emission scenario using CORDEX-CORE simulations. The work will be carried out for the near-future period as well as the middle-future period. The results of this study will help investors in the energy sector plan their investments in Côte d'Ivoire more carefully. To reach this aim, this paper is organized as follows: Section 2 presents the study area, the data, and the methodology. The results and discussions are summarized in Section 3. Finally, conclusions are given in Section 4.

2. Materials and Methods

2.1. Study Area

Côte d'Ivoire is located in West Africa along the Gulf of Guinea between 2°30′ and 8°30′ west longitudes and between 4°30′ and 10°30′ north latitudes (Figure 1). The country is approximately square in shape, and its southern border consists of a 515 km coastline along the Gulf of Guinea in the North Atlantic Ocean. It is divided into three climatically homogeneous zones based on weather and climate patterns [37–39]. These zones are the southern equatorial region (4–6° N), the central tropical region (6–8° N) and the northern semi-arid climatic region (8–10.5° N) (Figure 1). In Côte d'Ivoire, the regional climate is characterized by the north–south shift of the Intertropical Convergence Zone, which is

warm and humid, ranging from equatorial conditions along the southern coast to tropical conditions in the central regions and semi-arid conditions in the far north.

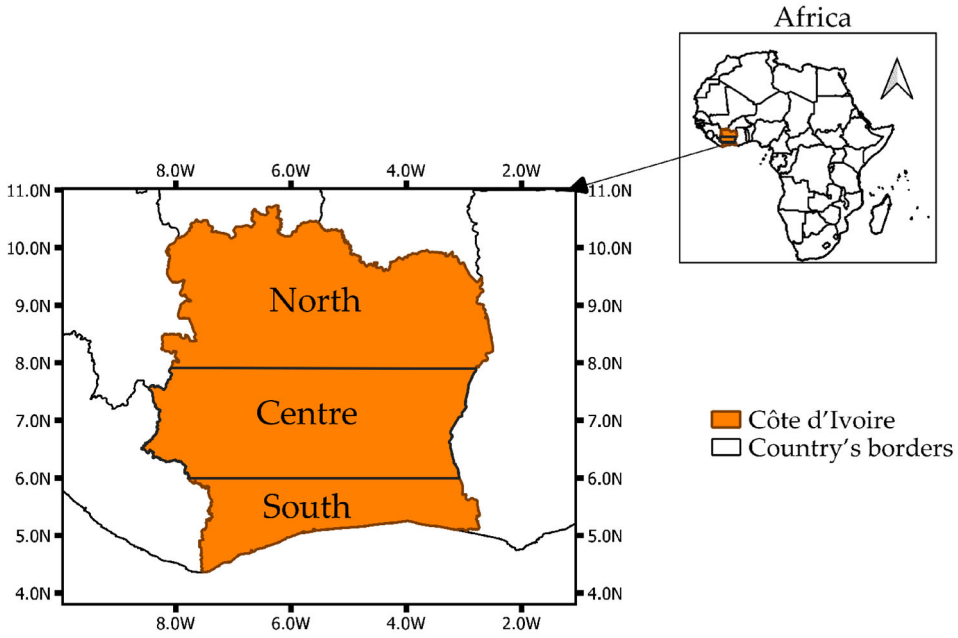

Figure 1. Geographical location of Côte d'Ivoire and climatic zones considered here based on the suggestion made by [37–39].

2.2. Data Used

2.2.1. Regional Climate Models

In this study, we quantify the impact of climate change on solar PV generation. To do this, we first downloaded two climate variables, namely, surface downwelling shortwave radiation (in W m^{-2}) and the near-surface air temperature (in °C), at a daily frequency from the CORDEX-CORE simulation over the entire Africa domain (Afri-22) with a spatial resolution of 0.22° by 0.22° (~25 km × 25 km) for the historical and future periods under the Representation Concentration Pathway (RCP) 8.5 scenarios. RCP8.5 is a rising pathway scenario (high-emission scenario), where the global mean temperature could reach a maximum of 4 °C by the end of the century. This scenario assumes that greenhouse gas emissions will lead to an equivalent CO2 concentration greater than 1000 ppm by 2100. Moreover, CORDEX-CORE provides high-resolution regional climate model (RCM) projections with greater detail and more accurate representation of localized events [40]. Many studies have demonstrated the accuracy of CORDEX-CORE models in providing consistent and high-resolution regional climate change projections [33,41–43].

The CORDEX-CORE models employed in this study are available on the Earth System Grid Federation (ESGF). They are based on three Regional Climate Models (RCMs), which include the German Climate Service Centre's REMO model, namely (REMO) [44], the Abdus Salam International Center for Theoretical Physics' RegCM4, namely (RegCM) [45], and the Consortium for Small-Scale Modeling (COSMO) community's CCLM (CCLM) [46]. The three RCMs are driven by three global climate models (GCMs), i.e., the Met Office Haley Centre Earth System model (HadGEM2-ES [47], the Max Planck Institute for Meteorology Earth System Model (MPI-ESM-MR [48], and the Norwegian Earth System Model (NorESM1-M [49], from the Coupled Model Intercomparison Project 5 (CMIP5 [50]). According to Giorgi et al. [45], these GCMs are among the best-performing models in the CORDEX domains within the CMIP5 ensemble. The simulation outputs are all from the

same ensemble members (i.e., realization, initialization, and perturbation 1; r1i1p1). The selected RCMs and their characteristics are summarized in Table 1.

Table 1. Parameterizations of the CORDEX-CORE models used in this study.

Regional Climate Model	Institute	Microphysics		Driving Model	Aerosol
RegCM4-	Abdus Salam International Center for Theoretical Physics (ITCP)	[51]	✔	MOHC-HadGEM2-ES	Organic and black carbon, SO_4 [52], dust [53], and sea salt [54].
CCLM	Consortium for Small-Scale Modeling (COSMO) community, the German Weather Service (DWD)	[55]	✔	MPI-M-MPI-ESM-LR	No aerosol module is included.
REMO	Climate Service Centre Germany (GERICS)	[56]	✔	NCC-NorESM1-M	No aerosol module is included. The information about aerosols, for example in the radiation scheme, is based on climatology [57]

We then compute the multi-model ensemble mean of each RCM (RegCM, REMO, and CCLM) and also the ensemble mean (Rmean) of all the models used. Rmean is calculated as the arithmetic mean of a variable from the nine models under CORDEX-CORE downloaded in this study.

2.2.2. Reference Datasets

In this work, two types of reference data were used. Firstly, air surface temperature (TAS) was downloaded from the fifth-generation global climate reanalysis (ERA5). ERA5 is a reanalysis product [58] of the European Centre for Medium-Range Weather Forecasts (ECMWF). It was developed by combining outputs from models and in situ data from meteorological stations across the globe [59]. ERA5 has a horizontal resolution of $0.25° \times 0.25°$ covering the period from 1979 to the present. ERA5 is a dataset that serves as the official validation database for the CORDEX models [60]. It is widely used in previous studies for model evaluation [30,33,61,62].

Finally, we used daily shortwave solar radiation retrieved from the Application Facility on Climate Monitoring (CM-SAF), specifically the second version of the Surface Solar Radiation Dataset-Heliosat Edition 2 (SARAH-2) [63,64] (see https://wui.cmsaf.eu; accessed on 31 January 2023). It is used for further model evaluation in numerous works [28,30,32,43]. SARAH-2 is a product derived from satellite observations of the visible channels of the MVIRI and SEVIRI instruments onboard the geostationary Meteosat satellites. The data are available from 983 to 2015 and have a spatial resolution of $0.05° \times 0.05°$.

2.3. Methodology

To understand the future impact of climate change on solar PV generation in Côte d'Ivoire, the RCMs used must realistically reproduce historical climate conditions. In the first step, we assessed the ability of CORDEX-CORE models to accurately reproduce the key climate variables (TAS and RSDS) used to compute solar PV potential during the reference period. Based on data availability, we used the period from 1986 to 2005 as the reference period for both observational datasets and climate model datasets.

To evaluate the simulated TAS and RSDS in the present day (1986–2005), we used surface temperature from the reanalysis dataset ERA5 and RSDS from the satellite-based climate dataset (SARAH-2). Further, it is noted that reanalysis datasets (ERA5) and satellite datasets (SAHRA-2 dataset) are used as substitutes and alternatives to ground observations in evaluating CORDEX-CORE models [62,65–67].

To address the difference in spatial resolution between the CORDEX-CORE simulations and the reference datasets, we used Climate Data Operators (CDO [68]) for remapping all the data to a common grid corresponding to the grid used by the fifth-generation global

climate reanalysis (ERA5), with a horizontal resolution (0.25° × 0.25°). The interpolation method used was bilinear interpolation, as in previous works [31,62]. In addition, we combined three statistical approaches: root mean square difference (RMSE), Pearson correlation coefficient (r), and mean absolute error (MAE) to evaluate the performance and consistency of the three RCMs and their ensemble mean over the study area. In addition, systematic biases between RCM simulations and observational data were also analyzed to evaluate the ability of the RCMs to reproduce the observed dataset. Afterwards, we analyzed the projected change through the difference between the estimated future values and their values in the reference period, considering the plausible greenhouse gas scenario RCP8.5. This high-emission pathway was chosen to assess the upper-bound climate response. Indeed, RCP8.5 enables clear, robust estimates of maximum projected changes, which are particularly relevant for climate risk assessment and adaptation planning.

In this section, the reference period, namely the historical period, spans 1986 to 2005. This reference period is widely used in many climate studies, such as [69,70]. We consider two future periods, namely the near future (2021–2040) and the middle future (2041–2060). The projected change is expressed as absolute changes for TAS and relative changes for RSDS and solar PV power potential with respect to the reference period. The statistical significance of projected changes in solar PV potential is assessed via the paired Wilcoxon signed-rank test. The null hypothesis assumes a median difference of zero, evaluated at a 95% confidence level ($p < 0.05$).

2.3.1. Estimation of Solar Photovoltaic Potential

The solar PV power output at a given site depends not only on its solar PV energy potential (PVpot) but also on the installed capacity. The instantaneous solar PV power production can be estimated by multiplying the solar PV potential by the nominal installed capacity. In this study, we estimate solar PV energy potential using the energy rating method, as in previous studies [28,31,71,72]:

$$\mathrm{PVpot} = \frac{\mathrm{PR(t)} \times \mathrm{RSDS(t)}}{\mathrm{RSDS_{STC}}} \tag{1}$$

where $\mathrm{RSDS_{STC}}$ represents the surface downwelling shortwave radiation under Standard Test Conditions (STCs), which equals 1000 $\mathrm{W/m^2}$. RSDS(t) is surface downwelling shortwave radiation at time (t), and PR indicates the performance ratio of the PV cells [31,71], expressed as follows:

$$\mathrm{PR(t)} = 1 + \gamma(\mathrm{T_{cell}(t)} - \mathrm{T_{STC}}) \tag{2}$$

where $\mathrm{T_{STC}} = 25\ ^{\circ}\mathrm{C}$ is the ambient air temperature under Standard Test Conditions (STCs). The constant γ depends on the physical parameters of the solar PV cell. In this study, we use a monocrystalline silicon solar cell (the most commonly used in Africa), for which γ takes the value of $(-0.005\ ^{\circ}\mathrm{C}^{-1})$ [28,71]. $\mathrm{T_{cell}}$ denotes the solar cell temperature, which depends on surface downwelling shortwave radiation, near-surface air temperature, and wind speed [73], and is calculated as follows:

$$\mathrm{T_{cell}(t)} = \mathrm{c_1} + \mathrm{c_2\ Tas(t)} + \mathrm{c_3\ RSDS(T)} + \mathrm{c_4 W_{10}(t)} \tag{3}$$

where $\mathrm{T_{cell}}$ is the ambient temperature around the cells (°C), RSDS is the surface downwelling shortwave radiation (W $\mathrm{m^{-2}}$), $\mathrm{W_{10}}$ is the wind speed (m $\mathrm{s^{-1}}$), and $\mathrm{c_1}$, $\mathrm{c_2}$, $\mathrm{c_3}$, and $\mathrm{c_4}$ are coefficients that depend on the PV material properties.

Recent studies have shown that the contribution of wind speed and relative humidity to changes in PVP is negligible in Africa [28,31]. Therefore, T_{cell} is expressed as a function of surface downwelling shortwave radiation (RSDS) and air temperature (TAS) as follows:

$$T_{cell}(t) = c_1 + c_2\,Tas(t) + c_3\,RSDS(T) \tag{4}$$

The coefficients c_1 = 3.75 °C, c_2 = 1.14, and c_3 = 0.0175 C m^2 W^{-1} for a monocrystalline silicon cell were taken from Lasnier and Ang [74] and used in [30,75].

Using Equations (1), (2) and (4), PVpot can be expressed as follows:

$$PVpot = \frac{RSDS(t) \times (1 + \gamma[(c_1 + c_2\,Tas(t) + c_3\,RSDS(t) - T_{STC})])}{RSDS_{STC}} \tag{5}$$

Considering a, b and c such that

$$a = \frac{(1 + \gamma(c_1 - T_{STC}))}{RSDS_{STC}} = 1.10625 \times 10^{-3}\ m^2 w^{-1}$$

$$b = \frac{\gamma c_2}{RSDS_{STC}} = -5.7 \times 10^{-6}\ m^2 w^{-1}/°C$$

$$c = \frac{\gamma c_3}{RSDS_{STC}} = -8.75 \times 10^{-8}\ m^4 w^{-2}$$

$$PVpot = RSDS(t)\ [a + bTas(t) + cRSDS(t)] \tag{6}$$

From Equation (5), we calculate the change in future solar PV potential relative to the historical period as follows:

$$\Delta PVpot = \frac{PVpot.fut - PVpot.his}{PVpot.his} \times 100\% \tag{7}$$

where PVpot.his and PVpot.fut are the historical and future solar PV potentials, respectively.

2.3.2. Evaluation Criteria for Model Performance

In this work, we combined three statistical approaches: root mean square difference (RMSE), Pearson correlation coefficient (r), and mean absolute error (MAE) to assess the performance and consistency of the three RCMs and their ensemble mean over the study area. All the statistical metrics used in this work are widely used in many studies to evaluate the performance of CORDEX-AFRICA-RCMs [31,76,77].

The Pearson correlation coefficient is a measure that shows the linear relationship between observations and model simulations. It ranges from −1 to 1, where −1 indicates a perfect negative correlation and 1 indicates a perfect positive correlation between the simulated model and the observed data [78,79]. The interpretation of the values of the Pearson correlation coefficient is based on Table 2 [80].

The mathematical formula of the Pearson correlation coefficient is:

$$r = \frac{\sum_{i=1}^{N} ((RCM_i - RCM_{avg}) \times (OBS_i - OBS_{avg}))}{\sqrt{\sum_{i=1}^{N} (RCM_i - RCM_{avg})^2 \sum_{i=1}^{N} (OBS_i - OBS_{avg})^2}} \tag{8}$$

The RMSE measures how accurately climate models simulate observed data.

Table 2. Pearson correlation coefficient (source: Evans [80]).

Pearson Correlation Coefficient	Relationship
0.00–0.19	very weak
0.20–0.39	weak
0.40–0.59	moderate
0.60–0.79	strong
0.80–1.00	very strong

It represents the distance between the means of climate models and those of the observed data. The smaller the value of RMSE, the better the model performance and vice versa [81,82]. The mathematical formula of RMSE is:

$$\text{RMSE} = \sqrt{\frac{\sum_{i=1}^{N}(\text{RCM}_i - \text{OBS}_i)^2}{N}} \quad (9)$$

The MAE is a calculation of the average absolute differences between the climate model and observed data. Similar to RMSE, the lower the value of MAE, the more accurate the model will be. The mathematical formula of MAE is given below:

$$\text{MAE} = \frac{\sum_{i=1}^{N}(|\text{RCM}_i - \text{OBS}_i|)}{N} \quad (10)$$

where RCM is the simulated model, OBS is the observed value at timestep i, and OBS_{avg} and RCM_{avg} are the corresponding average values for observed and simulated data, respectively. N is the total number of years.

3. Results and Discussion

3.1. Evaluation of Climate Models

In this section, we evaluate the capability of the RCMs and their ensemble mean to reproduce the spatial distributions and the mean annual cycle of TAS and RSDS, as well as the solar PV potential, during the historical period (1986–2005) over Côte d'Ivoire.

3.1.1. Annual Patterns of Climate Variables

Figures 2 and 3 present the simulated and observed spatial patterns of TAS and RSDS, respectively, during the reference period 1986–2005. All three RCMs, with their ensemble mean (Rmean), reproduce well the spatial distribution of TAS and RSDS over Côte d'Ivoire, with spatial correlations ranging from 0.79 to 0.89 for RSDS and from 0.65 to 0.93 for TAS. The analysis of the spatial distribution of TAS shows that the statistical metrics MAE and RMSE are close to zero (Figure 2). Indeed, the MAE is 0.29, 0.48, 0.51, and 0.64 for Rmean, RegCM, REMO, and CCLM, respectively. The RMSE is 0.36, 0.55, 0.75, and 0.76 for Rmean, RegCM, REMO, and CCLM, respectively. This confirms that the models Rmean, RegCM, REMO, and CCLM can practically simulate the spatial annual mean of near-surface temperature in Côte d'Ivoire. Rmean and RegCM performed better in simulating near-surface temperature than the other RCMs considered in this study. CCLM performed less well over the study area than the other RCMs. In agreement with observations, Rmean and RegCM showed the highest TAS values in the northern part of Côte d'Ivoire and the lowest in the southern part. The high temperatures in the northern part could be due to less vegetation cover in this region.

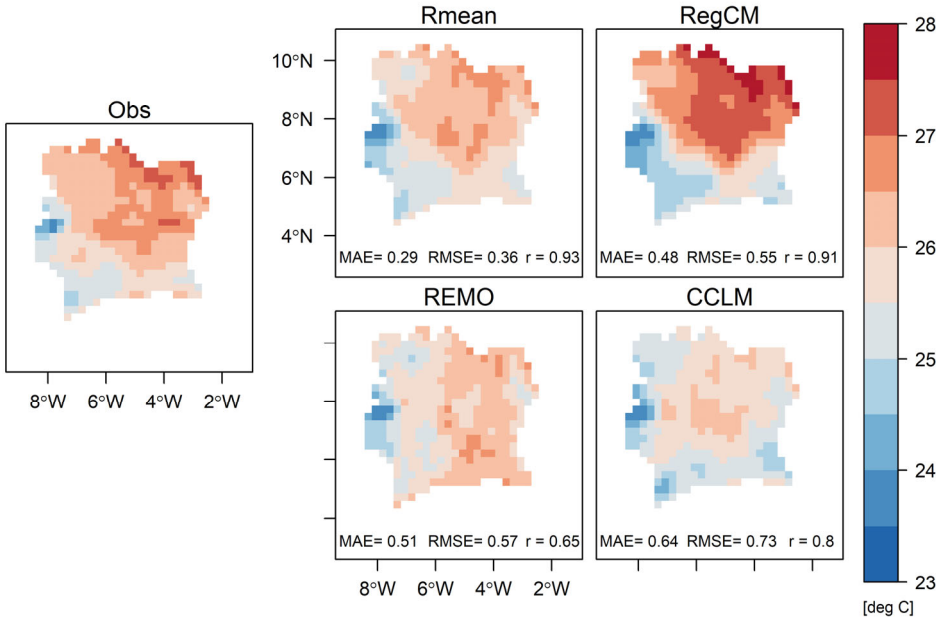

Figure 2. Mean annual patterns of near-surface air temperature (TAS) for the observational data, RCMs and their ensemble mean (Rmean) during the present climate (1986–2005) over Côte d'Ivoire. The mean absolute error (MAE), root mean square error (RMSE), and spatial correlation (r) between observations and simulations are indicated in the corresponding plots.

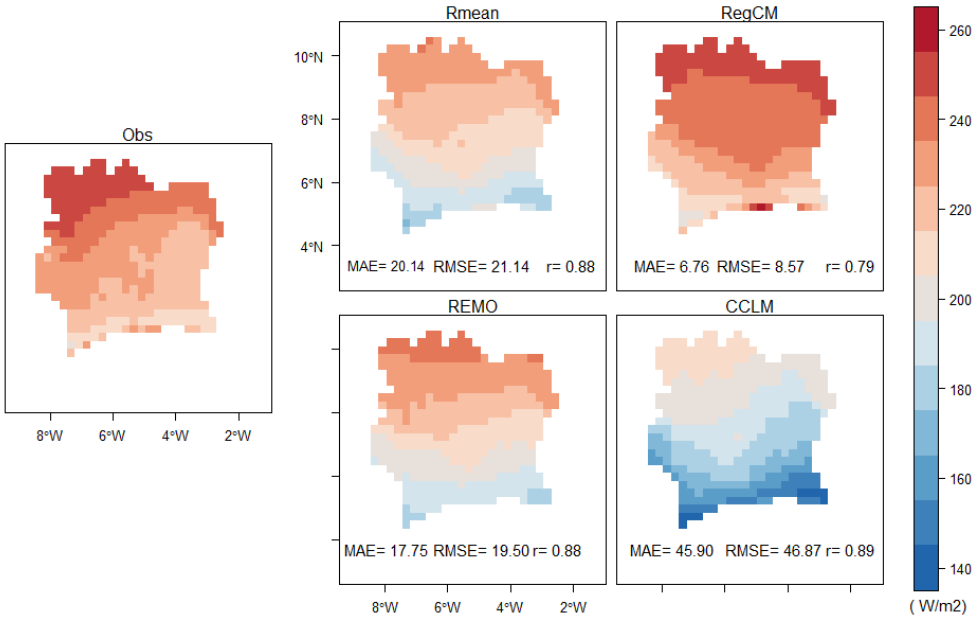

Figure 3. Similar to Figure 2, but for downwelling surface shortwave radiation (RSDS).

Referring to surface downwelling shortwave, as depicted in Figure 3, all the models show that RSDS gradually increases from the southern part to the northern part of Côte d'Ivoire, as observed. Indeed, the highest RSDS values occur in the northern part of Côte d'Ivoire, where most solar farms will be implemented in the future, followed by the central part of Côte d'Ivoire. Additionally, the lowest RSDS values are found in the southern part of Côte d'Ivoire. The north of Côte d'Ivoire generally experiences clear conditions, thereby having high values of RSDS. In contrast, the southern part of Côte d'Ivoire has lower RSDS values due to cloud cover throughout the year. From the statistical analysis, the RegCM model has the lowest MAE and RMSE, indicating that RegCM performs better than the other models in simulating RSDS over Côte d'Ivoire. Similar results have been found in

previous works [29,32]. According to Ndiaye et al. [33], the spatial distributions of the annual mean are captured by the RCMs as well as their ensemble mean in West Africa. It is also noticeable that RegCM4 performs well in TAS and RSDS in West Africa [30,33].

Despite the capability of the three RCMs and their ensemble mean to reproduce the observed spatial distributions of RSDS and TAS over Côte d'Ivoire, the analysis shows biases in the different variables across the study area (see Appendix A, Figures A1 and A2). For instance, Rmean, REMO, and CCLM underestimate RSDS over most parts of the study area. The magnitude of biases varies from −45.30 to −5.26 W/m^2, −43.77 to −2.077 W/m^2, and −81.64 to −28.78 W/m^2 for Rmean, REMO, and CCLM, respectively. The negative bias of RSDS is more important in the southern part of Côte d'Ivoire, while RegCM overestimates RSDS over most parts of Côte d'Ivoire, with biases ranging from −12.86 to 29.10 W/m^2. These biases related to RSDS may be attributed to cloud back-scattering or albedo and cloud absorption, but also to aerosols represented in climate models and the SARAH-2 datasets [30,83–85]. In addition, biases in RSDS could provide difficulties in representing clouds in climate models [62,86–88].

Concerning near-surface temperature, the results show that Rmean and CCLM underestimate the mean annual temperature of TAS in most parts of Côte d'Ivoire, with a prominent cool bias from north to south. Compared with the observations, there is a small bias ranging from −0.94 °C to 0.18 °C for Rmean and from −1.56 °C to 0.35 °C for CCLM over the study area. On the other hand, RegCM overestimates the annual mean TAS in the northern and most of the central parts of the study area but underestimates it in the southern part of Côte d'Ivoire. The biases range from –1.45 °C to 1.02 °C over the study area for RegCM. While REMO overestimates the annual mean TAS in the southern part of the study area, it underestimates it (from −1.24 °C to 0.81 °C) in the northern and central parts.

3.1.2. Annual Patterns of Solar PV Potential (PVpot)

Figure 4 describes the spatial distribution of the annual mean of observed and simulated PVpot with the three regional climate models (RCMs) and the ensemble mean (Rmean) during the period from 1986 to 2005 over Côte d'Ivoire.

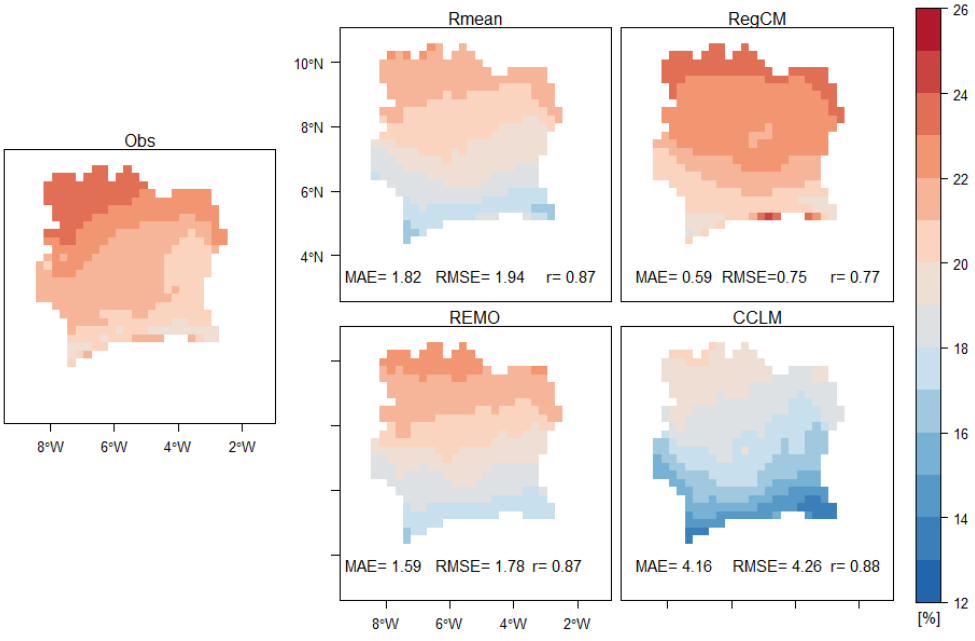

Figure 4. Similar to Figure 2, but for solar PV potential.

The analysis of Figure 4 shows that all three RCMs and the Rmean can capture well the spatial distribution of solar PV potential over Côte d'Ivoire, with a spatial correlation greater than 0.7 (0.87 for Rmean, 0.77 for RegCM, 0.87 for REMO and 0.88 for CCLM). This result is also shown by low RMSE values (1.94, 0.75, 1.78, and 4.26 for Rmean, RegCM, REMO, and CCLM, respectively) and low mean absolute errors (1.82, 0.59, 1.59, and 4.16 for Rmean, RegCM, REMO, and CCLM, respectively). These results align with previous works using observational data and climate models [33]. One can notice that the annual mean of PVpot decreases gradually from north to south across the models. The northern part of Côte d'Ivoire exhibits the largest PVpot, while the southern part of Côte d'Ivoire displays the smallest values.

It can be seen from Figures 3 and 4 that the spatial distribution of the annual mean PVpot is positively correlated with RSDS. This indicates that PVpot is primarily determined by RSDS. This result coincides with a study conducted in West Africa, where a strong positive correlation between RSDS and PVpot was found ($r > 0.93$) [31].

Despite the performance of the RCMs in reproducing the spatial distribution of the annual mean PVpot, there are some biases (see Appendix A, Figure A3). Indeed, Figure A3 shows that Rmean, REMO, and CCLM underestimate the annual mean of PVpot compared to the reference PVpot over Côte d'Ivoire, with biases ranging from −4.17% to −0.43% for Rmean, −4.09% to −0.12% for REMO, and −7.5% to −2.6% for CCLM. In contrast, RegCM overestimates PVpot in some parts of Côte d'Ivoire, such as the eastern north and eastern south, and underestimates it in other parts of the country. In general, the RegCM bias ranges from −1.3% to 2.8%.

3.1.3. Mean Annual Cycle of Climate Variables

In this section, the annual cycle averaged over the three homogeneous climatic zones (northern, southern, and central) of Côte d'Ivoire was examined to know the capability of all the models to reproduce the annual cycle of TAS, RSDS, and PVpot, as well as their minima and peaks (phase and amplitude), in the three climatic zones of Côte d'Ivoire.

Near-Surface Temperature (TAS)

Figure 5 illustrates the performance of the three RCMs (RegCM, REMO, and CCLM) and their ensemble mean (Rmean) in simulating the mean monthly near-surface temperature cycle over the three climatic subregions during the period 1986–2005. The data are monthly averages for the period 1986–2005. The results revealed that the three RCMs and their ensemble mean were good at representing the monthly pattern of observed air temperature across all climatic zones and the whole country. In fact, the monthly variation patterns of all the models are very similar to the observations. The maxima and minima of the TAS are well captured by these RCMs in the three climatic zones, with different magnitudes. All the models simulate the maximum TAS during the dry period of the year, from February to April. The minimum TAS is observed in August for all models. However, a few disagreements between the models and the observations can be highlighted. All the models underestimate the observed TAS from July to February and overestimate it from March to May in each climatic zone.

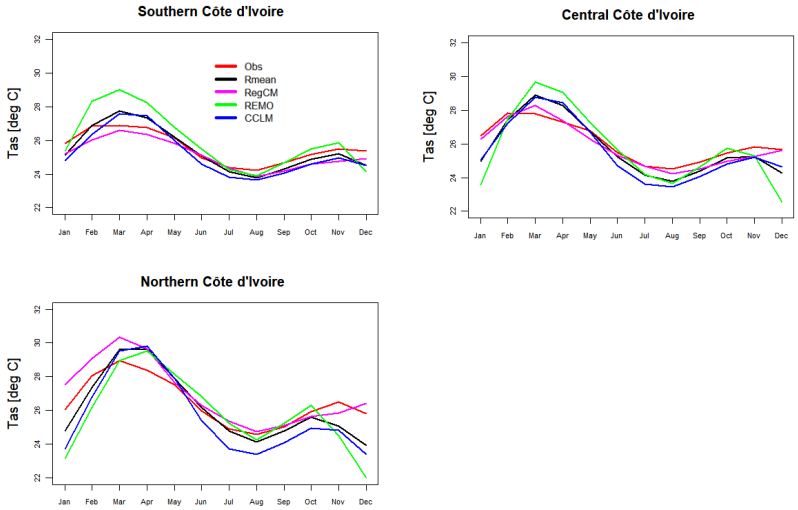

Figure 5. Mean annual cycle of near-surface air temperature in the observation data and simulated data (Rmean, RegCM, CCLM, and Rmean) over the three climatic zones for the period 1986–2005.

Annual Cycles of Monthly Climatology RSDS

Figure 6 represents the magnitude and distribution of the mean monthly observed and simulated (Rmean, RegCM, CCLM, and Rmean) output of RSDS over the three climatic zones for the period 1986–2005. The analysis of Figure 5 reveals that all the RCMs and the ensemble mean capture the annual cycle of solar radiation very well, including the peak, across the three climatic zones. In fact, all the models, in agreement with the observations, estimate the highest solar radiation (RSDS) during the dry period of the year, from February to March. The lowest solar radiation levels are estimated during the wet period, from June to September. The reduction in RSDS magnitude at this time of the year coincides with the rainfall season. The atmosphere at this time of year is largely moisture-laden, with abundant precipitation, clouds, and an overall increase in convective activity, reducing the amount of solar radiation reaching the ground. However, Figure 6 shows a few disagreements between the observation and the RCMs in all the climatic zones. For the RCMs (Rmean, RegCM and REMO), RSDS is predominantly overestimated from November to March and underestimated from April to October. CCLM underestimates RSDS throughout all months of the year across all regions.

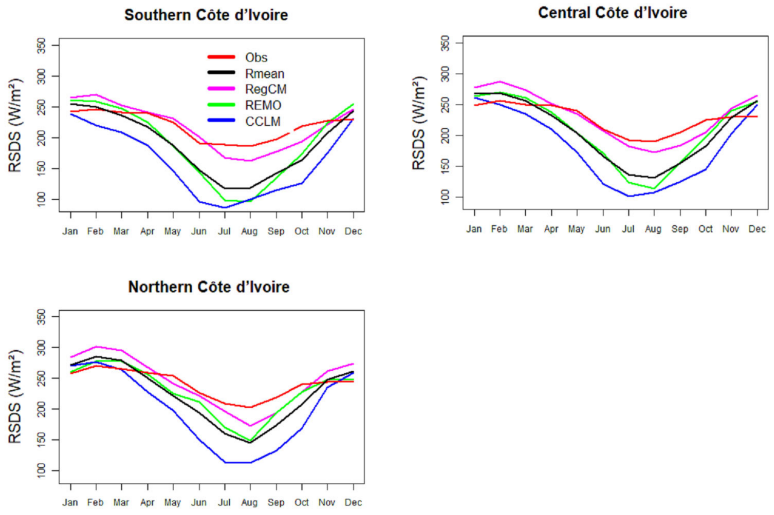

Figure 6. Similar to Figure 4, but for surface downwelling shortwave radiation (RSDS).

3.1.4. Mean Annual Cycle of Solar PV Potential (PVpot)

Figure 7 depicts the annual cycle of solar PV potential over the three climatic zones of Côte d'Ivoire during the period 1986–2005. It can be observed that the three RCMs and their ensemble mean capture the pattern of solar PV potential across all regions, indicating that all models reproduce the annual cycle of observed solar PV potential. The minimum solar PV potential is observed during the wet period from June to September. The maximum solar PV potential is estimated during the dry period of the year, from December to February. A similar pattern is also observed for solar radiation (Figure 6). The RCMs (RegCM and REMO) and Rmean underestimate PVpot from March to November and overestimate it from April to September. CCLM consistently underestimates PVpot in most months of the year, especially in the southern part of Côte d'Ivoire. Among the models, RegCM shows a better representation across the different areas. CCLM is the less efficient model for PVpot simulations.

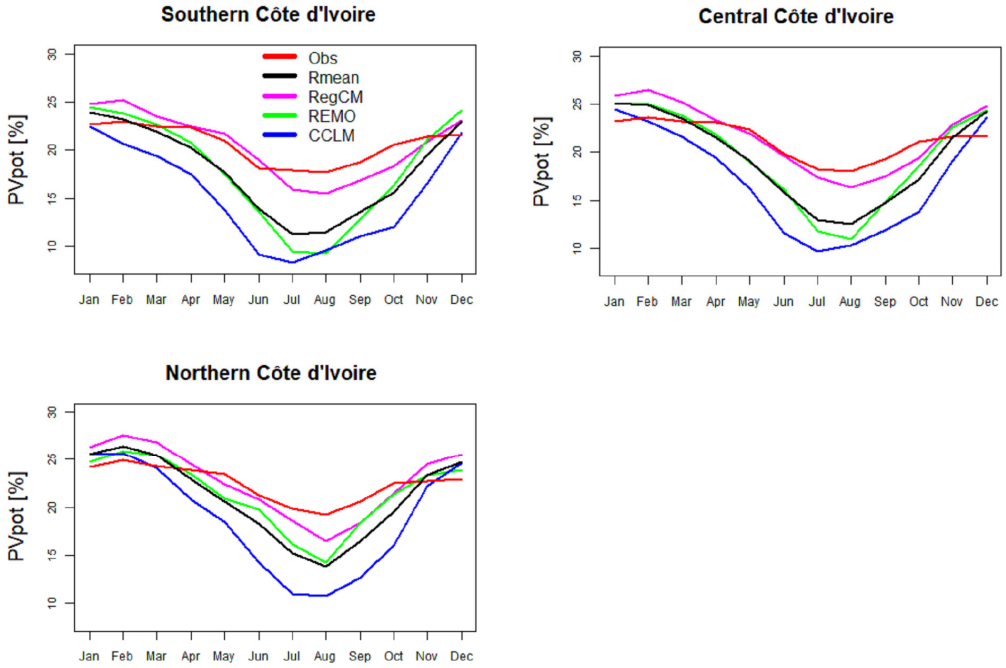

Figure 7. Similar to Figure 4, but for solar photovoltaic potential (PVpot).

3.2. Projection of Future Changes in Solar Photovoltaic Potential

In this section, we analyze the future projections of solar PV solar potential under the RCP8.5 scenario.

3.2.1. Changes in Future Annual Mean of Solar PV Energy Output

Herein, the climate change signal of the CORDEX-CORE models for the high-end scenario (RCP8.5) during the near-future and middle-future periods of solar PV generation is discussed.

Figure 8 shows the projected changes in solar PV potential for two future periods (near-future and middle-future) relative to the historical period in Côte d'Ivoire under the RCP8.5 scenario. As shown in Figure 7, the annual mean solar PV potential is projected to vary due to climate change across the country during both future periods. The analysis of Figure 8 reveals that all three RCMs (RegCM, REMO, and CCLM) and their ensemble mean (Rmean) project a general decrease in the annual mean solar PV potential during the near future relative to the historical period. In the near future, the average reduction is approximately 1.24%, 0.55%, 2.16%, and 1.05% for Rmean, RegCM, REMO, and CCLM,

respectively (Table 3). However, the magnitude of these changes depends on the climate model. The changes in the annual mean solar PV potential relative to the historical period range from −2.42% to −0.74% (Rmean), from −1.71% to 0.07% (RegCM), from −3.37% to −1.52% (REMO), and from −2.86% to −0.07% (CCLM). One can observe that RegCM presents a moderate decrease in solar PV potential compared to the other models in the near-future period. Moreover, the spatial distribution of these expected changes in solar PV potential is similar for all the models across Côte d'Ivoire but differs in terms of magnitude. All models show a clear south–north gradient, with the highest decrease located in the southern part of Côte d'Ivoire. In some parts of this region, the changes in solar PV potential reach up to −1% for RegCM and approximately −3% for the other models (Rmean, REMO, and CCLM) in the near future. The smaller decrease is located in the northern part of Côte d'Ivoire, with around −0.7% for Rmean and 1.5% for REMO. We can also observe a negligible decrease in some places in the north with CCLM and RegCM (−0.07%).

Table 3. Average changes in solar PV potential (%) during the near future and the middle future under the RCP8.5 scenario relative to the historical period (1986–2005) over Côte d'Ivoire.

	Rmean	RegCM	REMO	CCLM
Middle-future	−2.14	−1.559	−3.456	−1.3647
Near-future	−1.2361	−0.5524	−2.162	−1.0461

Concerning the middle future, all the models present similar signs of changes in the annual mean of solar PV potential to those in the near future, except CCLM, which shows a slight increase in some areas of the northern part of Côte d'Ivoire (around 0.03%). The projected changes in solar PV potential vary between −4.17% and −2.14%, −3.40% and −1.56%, and −4.63% and −1.36% for Rmean, RegCM, REMO, and CCLM, respectively. From the results, it can be noted that the reduction in solar PV potential will be stronger in the middle future across the country. Indeed, the average reduction in the annual mean solar PV potential over the whole Côte d'Ivoire is around −2% for Rmean, −1.6% for RegCM, −3.5% for REMO, and −1.4% for CCLM in the middle future (Table 3).

As in the near future, the spatial distribution of projected solar PV potential changes relative to the historical period is characterized by the south–north gradient during the middle future. In that future period, the southern part of the region is also projected to experience the most pronounced reduction in solar PV potential with values up to 4%, 3%, 5%, and 4.6% for Rmean, RegCM, REMO, and CCLM, respectively.

Furthermore, analysis of the 25th and 75th percentiles across the RCM ensemble under RCP8.5 (see Appendix A, Figure A4) reveals that both quartiles remain negative throughout the study area. This consistency across the interquartile range underscores robust agreement among the RCMs regarding the projected decline in annual average solar PV potential.

On the other hand, Figure 9 displays predominantly negative changes in solar PV potential across all RCMs and their ensemble mean under RCP8.5. The near- and middle-future periods exhibit median values below zero for all the simulated RCMs. This demonstrates a projected reduction in solar PV potential over the study area relative to the reference period. The decline appears more pronounced in the middle future, suggesting a gradual intensification of the signal toward the late century. Although inter-model variability is evident, the general agreement among the model outputs regarding the negative direction change increases confidence in the robustness of the projected decline of annual mean solar PV potential over Côte d'Ivoire. Moreover, the wider interquartile range in the middle future indicates increasing uncertainty in long-term projections.

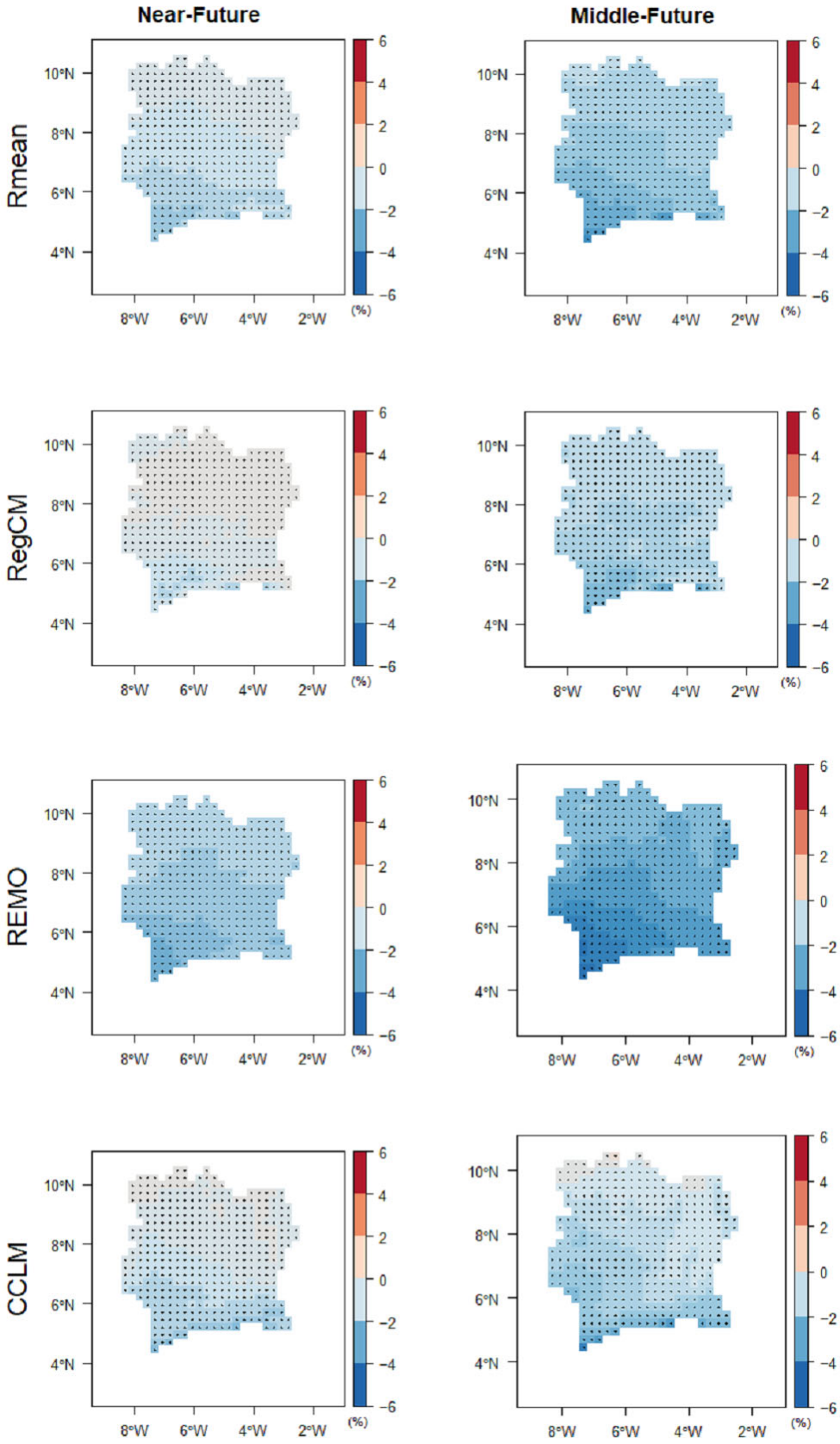

Figure 8. Annual potential solar photovoltaic power generation change (%) for the near future (2021–2040) and middle future relative to the historical period (1986–2005) under the RCP-8.5 scenario. Statistically significant areas are indicated with black dots.

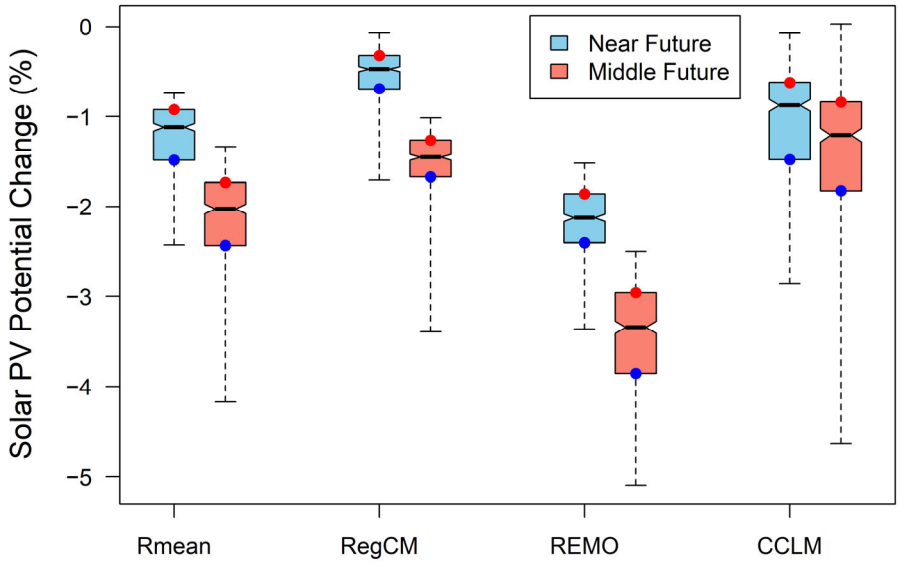

Figure 9. Box-and-whisker plots of the projection changes in solar PV potential for the RCMs (Rmean, RegCM, REMO and CCLM) during the near and middle future relative to the historical period (1986–2005) under the RCP8.5 scenario. The model median is indicated by the center line in the box plots. The red and blue dots represent the 75th and 25th percentiles, respectively. The black lines indicate the medians.

The reduction in future solar PV potential over Côte d'Ivoire found in this work is in line with previous studies that examined the adverse impact of climate change on solar energy generation over West Africa [27,31,33] and even across the entire African continent [28,30,32]. They found that solar PV potential is projected to decrease over West Africa in the future. The magnitude of the decrease varies among researchers; this difference may be due to the method used to compute the solar cell temperature, the future period used, and the climate model used. For instance, Sawadogo et al. [31] showed that the maximum decrease in photovoltaic power generation potential is less than 3.8% over any country in West Africa under the RCP 8.5 scenario using 14 RCM simulations from the Coordinated Regional Climate Downscaling Experiment (CORDEX) at 50 km resolution. With the RegCM CORDEX-CORE, solar PV potential is projected to decrease by up to 2% over the African continent in the mid-century period under the RCP8.5 scenario, as reported by Sawadogo et al. [30]. Ndiaye et al. [33] also found that the future solar PV potential could reduce from ~−2 in the near future to −4% in the far future using CORDEX-CORE data. In contrast, Danso et al. [27] indicate a larger decline in solar PV potential of up to 12% using CMIP6 models. The general reduction in solar PV potential observed across Côte d'Ivoire could be attributed to changes in RSDS and TAS induced by accelerating warming under a business-as-usual scenario, as suggested in previous studies [30,31,33]. These findings underscore the importance of incorporating climate change impacts into long-term solar PV energy planning.

3.2.2. Changes in Future Mean Annual Cycles of Solar PV Energy Output

Figure 10 presents the mean annual cycle of future solar PV potential changes in the near and middle future under the RCP8.5 scenario. In both future periods, all models agree on the seasonal evolution of solar PV potential changes across all climatic zones of Côte d'Ivoire. However, the magnitude of change varies across months. In general, all models project weak changes in solar PV potential from December to May over the three climatic zones for both future periods. The largest solar PV changes are observed from June to November across the three climatic zones in both future periods.

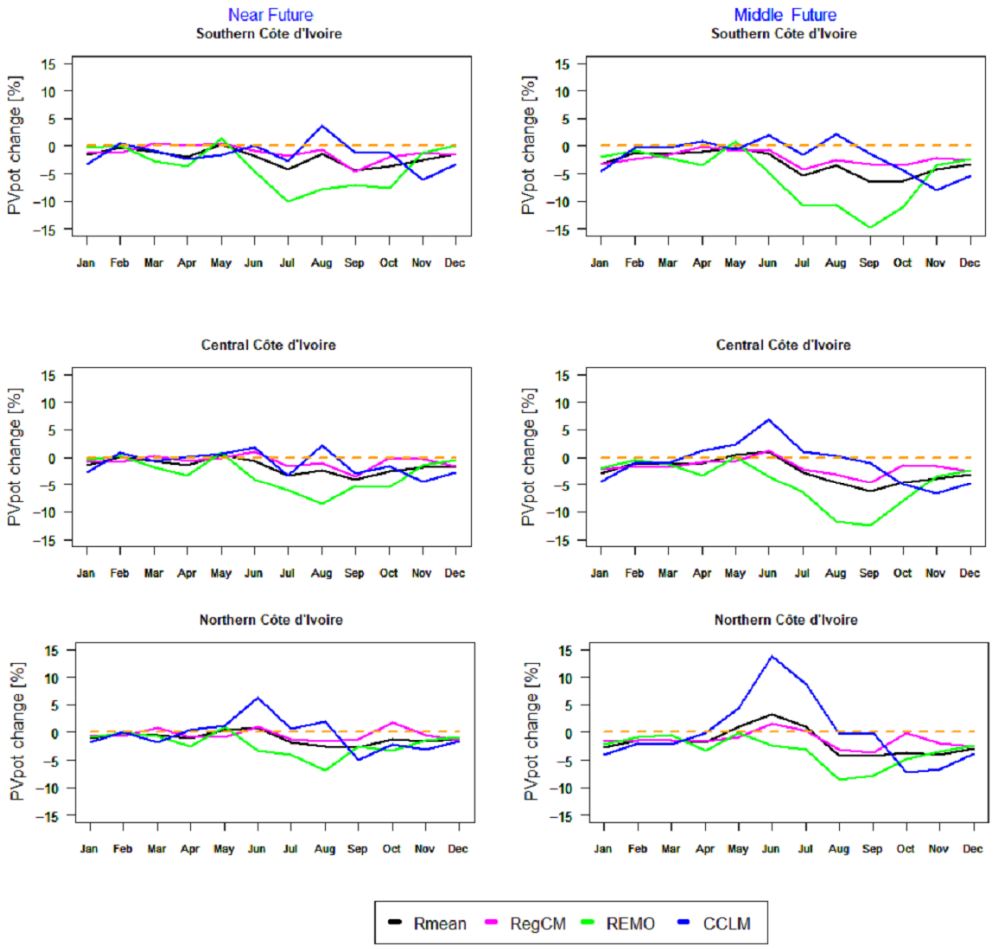

Figure 10. Relative changes in the mean annual cycle of solar PV potential for the near future (2021–2040) and the middle future relative to the historical period (1986–2005) under the climate scenario RCP-8.5 in the three climatic zones of Côte d'Ivoire. The orange dashed indicates no change relative to the historical period.

In the near future, the reduction in solar PV potential from June to October could reach about −4.5% for Rmean and RegCM, −10% for REMO, and −6% for CCLM in the southern part of Côte d'Ivoire. In the central part of Côte d'Ivoire, this decrease is around −3.9% for the models (Rmean, RegCM, and CCLM) and −8.5% for REMO. In the northern part, the decrease in the change in solar PV potential is around −2% for Rmean and RegCM, −6% for REMO, and −4.9% for CCLM.

In the middle future, solar PV potential changes are predominantly negative throughout the year, with larger decreases during the period from June to November in all climatic zones. The highest decrease in solar PV potential could reach up to −6%, −4%, −14%, and −7% in the south of Côte d'Ivoire with Rmean, RegCM, REMO, and CCLM, respectively. In the central part of Côte d'Ivoire, the decrease could be up to −6%, −4.5%, −12.5%, and −6.7% with Rmean, RegCM, REMO, and CCLM, respectively. In the northern part of Côte d'Ivoire, the decrease in solar PV potential is up to −4.2%, −3.5%, −8.6%, and −7% with Rmean, RegCM, REMO, and CCLM, respectively.

The analysis of Figure 8 reveals that the smaller decrease in future solar PV potential seems to be in the north of Côte d'Ivoire. The highest decrease is located in the southern part of Côte d'Ivoire, especially from June to October. Moreover, the annual cycle of future PV change does not always have negative values throughout the year. Some models project a slight increase in solar PV potential in the near and middle future. For instance, during the near-future period, positive changes could be seen in May (up to 1.35% for REMO

and 0.25% for Rmean) and August (up to 3.5% for CCLM) in the southern part of Côte d'Ivoire. During the middle-future period, REMO projects an increase in May (up to 0.85%), while CCLM projects increases in June and August (up to 2%) in the same climatic zone. In the central zone, slight increases could be observed in the near future in June (up to 1.75% and 1% for CCLM and RegCM, respectively) and August (up to 2.15% for CCLM). Furthermore, increases of about 1% and 7% could be projected in June for the models (Rmean and RegCM), and for CCLM, respectively. In the north of Côte d'Ivoire, increases are projected from May to July with CCLM during the near future and with RegCM, Rmean, and CCLM during the middle future.

These results generally agree with the findings of Danso et al. [27]. They pointed out that solar PV potential production is projected to decrease highly from June to October, with changes of up to about −15% (−7%) and −11% (−5%) during the far future (near future) in the Guinea area of West Africa under the SSP5-8.5 scenario using CMIP6 climate models.

4. Conclusions

This study quantified how future solar PV potential output in Côte d'Ivoire is likely to change by the mid-21st century under the RCP8.5 scenario. To achieve this target, this study utilized three regional climate models from CORDEX-CORE simulation over the African domain and the ensemble mean of the RCMs, which is widely used for climate change impact studies in Africa. The projected changes were carried out for the near future (2021–2040) and the middle future (2041–2060) relative to the baseline period (1986–2005). We began this study by evaluating the abilities of RCMs and their ensemble mean in simulating TAS, RSDS, and PVpot over Côte d'Ivoire. The main findings of this study can be summarized as follows:

- Rmean, RegCM, REMO, and CCLM were able to capture the observed annual cycle and spatial patterns of TAS, RSDS, and PVpot, but with some biases.
- The overall solar PV potential is predicted to decline slightly in Côte d'Ivoire during the mid-21st century due to the impacts of climate change.
- In the near future, the annual decrease is, on average −1.24%, −0.55%, −2.16%, and −1.05% for Rmean, RegCM, REMO, and CCLM, respectively. In the middle future, Côte d'Ivoire is projected to experience a large decrease in solar PV potential, on average −2% for Rmean, −1.6% for RegCM, −3.5% for REMO, and −1.4% CCLM. In addition, for both future periods, this reduction could be more noticeable during the months from June to October across all climatic zones, with different magnitudes.
- It is noted that the southern region of Côte d'Ivoire is the most affected by this decrease in solar PV potential. In contrast, a slight decrease in solar PV potential is found in the northern part of Côte d'Ivoire.

Regarding the impact of climate change on the future reliability of solar PV potential in Côte d'Ivoire, it will be useful to develop robust plans to successfully integrate solar energy into the power grid (off-grid and grid-connected systems), such as identifying synergies with other energy sources (example: hydropower, fossil fuels, and biomass) and investing in energy storage systems in order to increase the flexibility of power systems.

This study provides useful information on the impact of climate change on solar PV energy production in Côte d'Ivoire. The foundation of this work could help policymakers and stakeholders build strategies for climate change adaptation and plan large-scale solar energy projects in Côte d'Ivoire. However, the current projections could be improved in several ways: (1) Our results are based on a single scenario, the RCP8.5 scenario, the business-as-usual scenario, to predict future solar PV potential. It is therefore important to also explore the future outlook of solar PV potential under other climate scenarios

(i.e., other RCPs or shared socio-economic pathways (SSPs)). (2) Future studies could also assess the robustness of the projected change in solar energy from CORDEX-CORE over the study area. (3) Aerosols and clouds are well known to be strong modulators of solar radiation. Therefore, it may be useful to assess the combined effect of clouds and dust on solar irradiance in the study area. (4) Future work should incorporate aerosol–climate interactions and dynamic dust modeling to better constrain PV projections in West Africa. (5) Several large-scale solar power plants will be located in the northern part of Côte d'Ivoire in the coming years. Thus, future work may investigate future solar PV potential by focusing on regions where major solar power plants are located. Nevertheless, the results of this study provide useful information for sustainable energy planning using PV technologies in Côte d'Ivoire.

Author Contributions: Conceptualization, N.A.E.J.K.; Methodology, N.A.E.J.K., W.S. and A.J.A.; Software, N.A.E.J.K.; Validation, N.A.E.J.K., A.J.A., W.S., Y.M., B.A. and S.M.; Formal Analysis, N.A.E.J.K., W.S., A.J.A., B.A. and S.M.; Investigation, N.A.E.J.K., W.S., A.J.A., B.A. and Y.M.; Data Curation, N.A.E.J.K. and W.S.; Funding Acquisition, N.A.E.J.K.; Writing—Original Draft Preparation, N.A.E.J.K. and W.S.; Writing—Review and Editing, N.A.E.J.K., W.S., A.J.A., B.A., Y.M. and S.M.; Supervision, W.S., S.M., B.A., A.J.A. and Y.M. All authors have read and agreed to the published version of the manuscript.

Funding: This publication was financially supported by the German Ministry for Education and Research (BMBF) through the West African Science Service Center on Climate Change and Adapted Land Use (WASCAL) program.

Data Availability Statement: The data presented in this study are openly available at https://esg-dn1.nsc.liu.se/search/cordex/ (accessed on 31 January 2023); https://cds.climate.copernicus.eu/datasets/reanalysis-era5-single-levels?tab=download (accessed on 31 January 2023); https://wui.cmsaf.eu/safira/action/viewDoiDetails?acronym=SARAH_V002 (accessed on 31 January 2023).

Acknowledgments: We would like to express our gratitude to the modeling groups for computing and providing the RCM simulations in the frame of the Coordinated Regional Downscaling Experiment (CORDEX) Framework and COmmon Regional Experiment (CORE). We are also grateful to the European center for Medium-Range Weather Forecast (ECMWF) for providing the ERA5 reanalysis products. The authors acknowledge the provision of surface solar radiation by the Satellite Application Facility on Climate Monitoring (CM SAF). Finally, the authors would like to thank the anonymous reviewers for their thorough revision of the manuscript, which significantly improved the paper's quality.

Conflicts of Interest: The authors declare that the research was conducted in the absence of any commercial or financial relationships that could be construed as a potential conflict of interest.

Abbreviations

The following abbreviations are used in this manuscript:

AR5	Fifth Assessment Report
CDO	Climate Data Operators
CM SAF	Satellite Application Facility on Climate Monitoring
CMIP5	Climate Model Intercomparison Project Phase 5
CMIP6	Climate Model Intercomparison Project Phase 6
CORDEX	Coordinated Regional Climate Downscaling Experiment
CORE	Common Regional Experiment
ECMWF	European Centre for Medium-Range Weather Forecasts
GCMs	General climate models
HadGEM2-ES	Hadley Center Global Environment Model Version 2 Met Office Haley Centre Earth System Model

IPCC	Intergovernmental Panel on Climate Change
MAE	Mean absolute error
MPI-ESM-MR	Max Planck Institute for Meteorology Earth System Model
MVIRI	Meteosat Visible and InfraRed Imager
NorESM1-M	Norwegian Earth System Model
OBS	Observation value
PR	Performance ratio of solar photovoltaic cells
PV	Photovoltaic
PVpot	Solar photovoltaic power generation potential
r	Pearson correlation coefficient
RCM	Regional climate model
RCP	Representative Concentration Pathway
RegCM4	Regional climate model version 4
RMSE	Root mean square error
RSDS	Surface downwelling shortwave radiation
SARAH-2	Surface Solar Radiation Data Set—Heliosat Edition 2
SEVIRI	Spinning Enhanced Visible and InfraRed Imager
SSPs	Shared socio-economic pathways
STC	Standard test conditions
TAS	Near-surface air temperature
T_{Cell}	Solar cell temperature
T_{STC}	Ambient air temperature at standard test conditions
UNFCCC	United Nations Framework Convention for Climate Change
W_{10}	Wind speed at 10 m above the ground
WASCAL	West African Science Service Center on Climate Change and Adapted Land Use

Appendix A

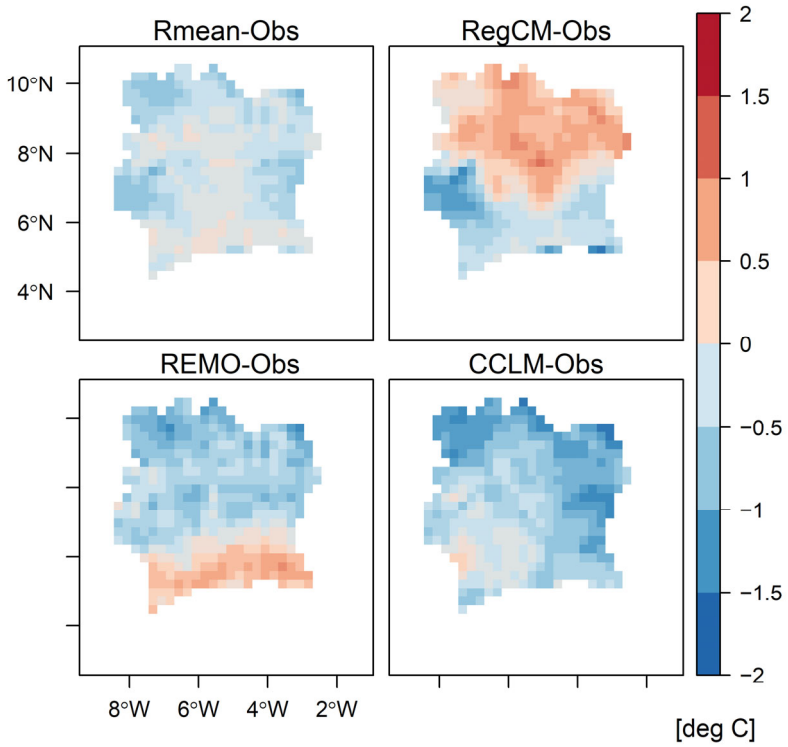

Figure A1. Bias maps (simulations minus observations) for the climatological mean of annual TAS for the models RegCM, REMO, CCLM, and Rmean in comparison with ERA5 TAS data during the period 1986–2005 over Côte d'Ivoire.

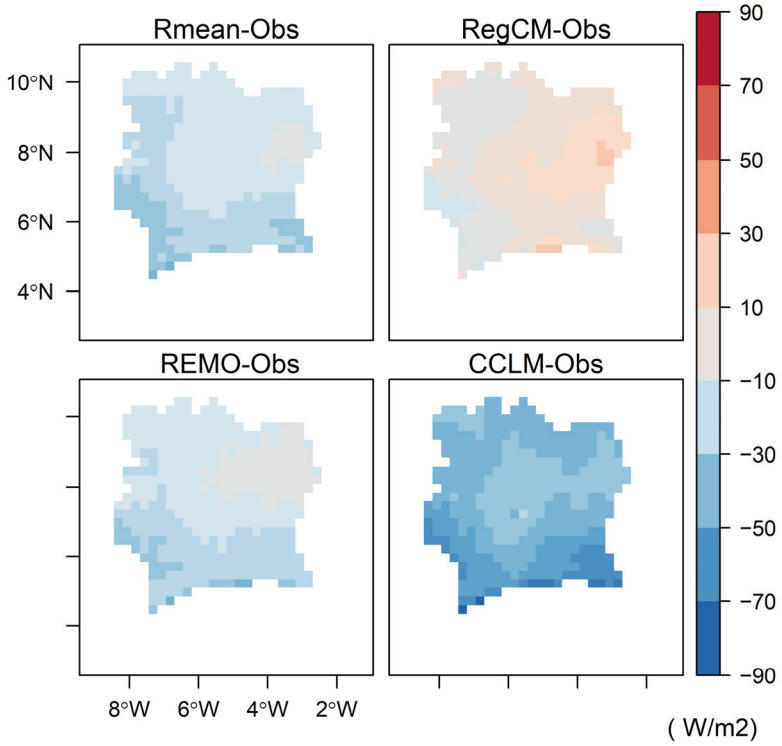

Figure A2. Bias maps (simulations minus observations) for the climatological mean of annual RSDS for the models RegCM, REMO, CCLM, and Rmean in comparison with SARAH-2.1 data during the period 1986–2005 over Côte d'Ivoire.

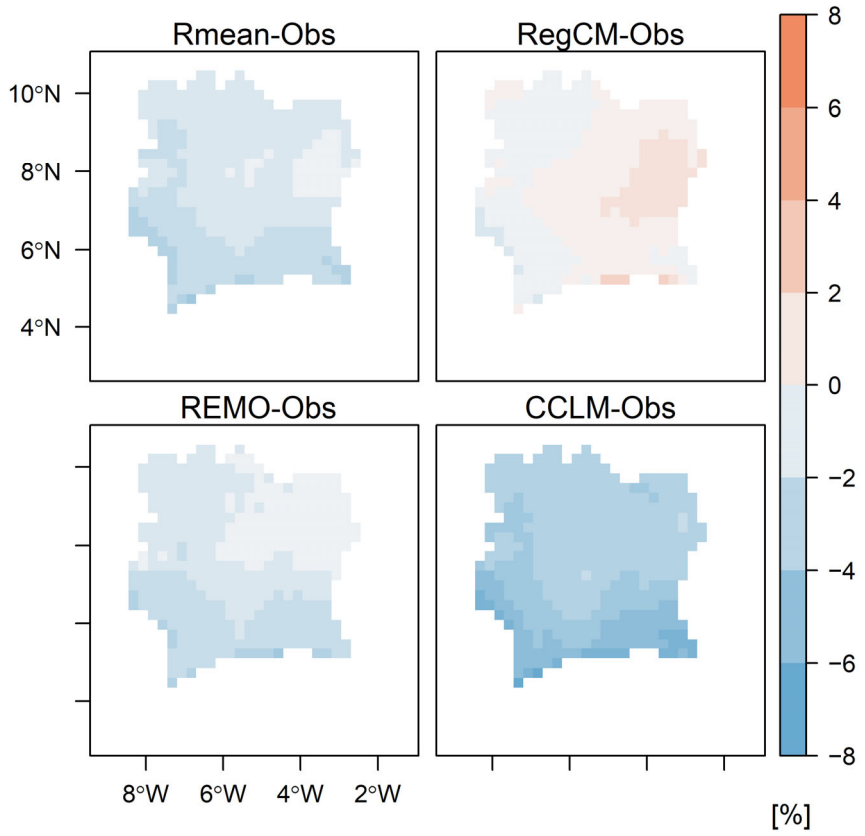

Figure A3. Bias maps (simulations minus observations) of the annual mean of solar PV power potential (PVpot) during the present climate (1986–2005) of the models RegCM, REMO, CCLM, and their ensemble mean (Rmean).

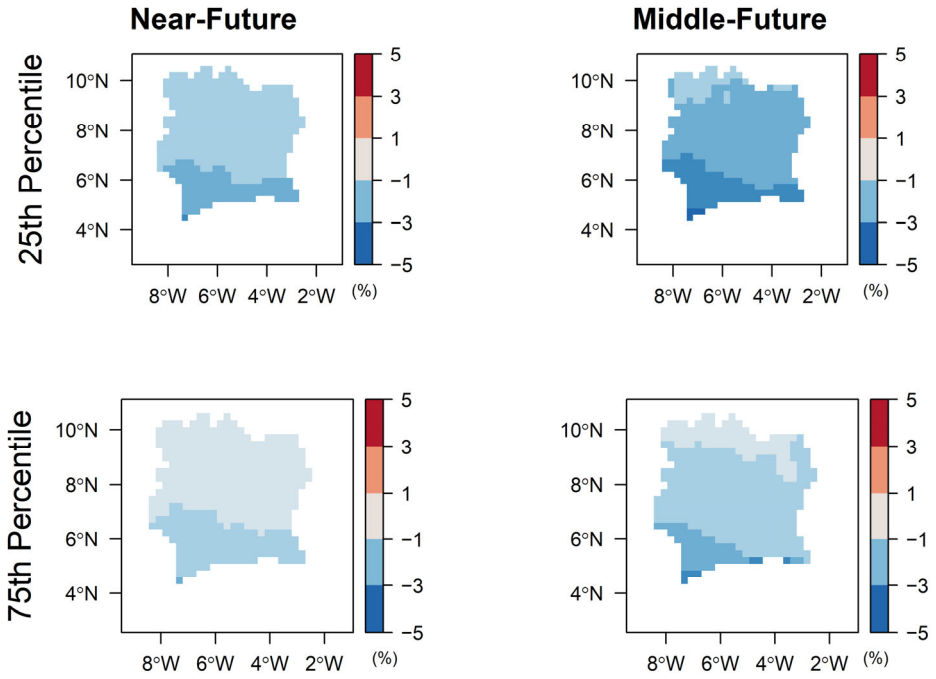

Figure A4. Spatial distribution of the 25th and 75th percentile projected change in solar PV potential (%) for the near- and middle-future period relative to the historical period 1986–2005, derived from the RCMs (RegCM, REMO, and CCLM.

References

1. Watts, N.; Amann, M.; Arnell, N.; Ayeb-Karlsson, S.; Beagley, J.; Belesova, K.; Boykoff, M.; Byass, P.; Cai, W.; Campbell-Lendrum, D.; et al. The 2020 Report of The Lancet Countdown on Health and Climate Change: Responding to Converging Crises. *Lancet Lond. Engl.* **2021**, *397*, 129–170. [CrossRef]
2. Mora, C.; Spirandelli, D.; Franklin, E.C.; Lynham, J.; Kantar, M.B.; Miles, W.; Smith, C.Z.; Freel, K.; Moy, J.; Louis, L.V.; et al. Broad Threat to Humanity from Cumulative Climate Hazards Intensified by Greenhouse Gas Emissions. *Nat. Clim. Change* **2018**, *8*, 1062–1071. [CrossRef]
3. Ezeife, N.D. Projected Impact of Global Warming on West Africa: Case for Regional and Transnational Adaptive Measures. *Annu. Surv. Int. Comp. Law* **2014**, *20*, 9.
4. Nations, U. Causes and Effects of Climate Change. Available online: https://www.un.org/en/climatechange/science/causes-effects-climate-change (accessed on 21 December 2025).
5. Crippa, M.; Guizzardi, D.; Pagani, F.; Banja, M.; Muntean, M.; Schaaf, E.; Quadrelli, R.; Risquez Martin, A.; Taghavi-Moharamli, P.; Köykkä, J.; et al. *GHG Emissions of All World Countries: 2025*; Publications Office of the European Union: Luxembourg, 2025; ISBN 978-92-68-31401-2.
6. Yeo, W.M. A Political Economy Analysis of the Electricity Sector in Côte d'Ivoire. *Energy Res. Soc. Sci.* **2024**, *118*, 103833. [CrossRef]
7. IRENA. Côte d'Ivoire. Available online: https://www.irena.org/-/media/Files/IRENA/Agency/Statistics/Statistical_Profiles/Africa/Cote-d-Ivoire_Africa_RE_SP.pdf(accessed on 12 March 2025).
8. Calvin, K.; Dasgupta, D.; Krinner, G.; Mukherji, A.; Thorne, P.W.; Trisos, C.; Romero, J.; Aldunce, P.; Barrett, K.; Blanco, G.; et al. *IPCC, 2023: Climate Change 2023: Synthesis Report. Contribution of Working Groups I, II and III to the Sixth Assessment Report of the Intergovernmental Panel on Climate Change*; Core Writing Team, Lee, H., Romero, J., Eds.; Intergovernmental Panel on Climate Change (IPCC): Geneva, Switzerland, 2023.
9. The Paris Agreement | UNFCCC. Available online: https://unfccc.int/process-and-meetings/the-paris-agreement (accessed on 22 December 2025).
10. Maslin, M.A.; Lang, J.; Harvey, F. A Short History of the Successes and Failures of the International Climate Change Negotiations. *UCL Open Environ.* **2023**, *5*, e059. [CrossRef]
11. UNFCCC Secretariat. Report of the Conference of the Parties on Its Twenty-First Session, Held in Paris from 30 November to 11 December 2015. In *Addendum. Part Two: Action Taken by the Conference of the Parties at Its Twenty-First Session*; UNFCCC Secretariat: Bonn, Germany, 2016.
12. International Renewable Energy Agency. *Future of Solar Photovoltaic: Deployment, Investment, Technology, Grid Integration and Socio-Economic Aspects*; International Renewable Energy Agency: Abu Dhabi, Saudi Arabia, 2019; ISBN 978-1-5231-5186-8.

13. Sterl, S.; Vanderkelen, I.; Chawanda, C.; Russo, D.; Brecha, R.J.; Griensven, A.; Lipzig, N.; Thiery, W. Smart Renewable Electricity Portfolios in West Africa. *Nat. Sustain.* **2020**, *3*, 710–719. [CrossRef]
14. Abudu, H.; Wesseh, P.K.; Lin, B. Are African Countries on Track to Achieve Their NDCs Pledges? Evidence from Difference-in-Differences Technique. *Environ. Impact Assess. Rev.* **2023**, *98*, 106917. [CrossRef]
15. Contributing to Enhance Côte d'Ivoire's Commitment to Climate Change Mitigation. Available online: https://idh.org/news/contributing-to-enhance-cote-divoires-commitment-to-climate-change-mitigation (accessed on 20 November 2025).
16. Open Knowledge Repository. Available online: https://openknowledge.worldbank.org/entities/publication/33cc2173-b868-5b15-b46c-3e3aa1025c7a (accessed on 20 November 2025).
17. Renewable Energy and Biomass in Côte d'Ivoire | EDF Ivory Coast. Available online: https://cotedivoire.edf.com/en/our-activities/renewable-energy-and-biomass-in-cote-d-ivoire (accessed on 20 November 2025).
18. IRENA. The Renewable Energy Transition in Africa. Available online: https://www.irena.org/-/media/Files/IRENA/Agency/Publication/2021/March/Renewable-Energy-Transition-Africa_Country_Studies_2021.pdf (accessed on 12 April 2025).
19. IEA. *IEA Renewables 2025*; IEA: Paris, France, 2025. Available online: https://www.iea.org/reports/renewables-2025 (accessed on 22 December 2025).
20. Clauzel, L.; Anquetin, S.; Lavaysse, C.; Tremoy, G.; Raynaud, D. West African Operational Daily Solar Forecast Errors and Their Link with Meteorological Conditions. *Renew. Energy* **2024**, *224*, 120101. [CrossRef]
21. Ivory Coast Solar Panel Manufacturing | Market Report. Available online: https://www.pvknowhow.com/solar-report/ivory-coast/ (accessed on 12 April 2025).
22. News, A.D. *Côte d'Ivoire Approves Major Solar Projects to Boost Renewable Energy Capacity*; Africa Digest News: Lyon, France, 2024.
23. Euroconvention Glob. *Renpower Côte d'Ivoire*, 3rd ed.; Euroconvention Glob: Brussels, Belgium, 2024.
24. Dajuma, A.; Yahaya, S.; Touré, S.; Diedhiou, A.; Adamou, R.; Konaré, A.; Sido, M.; Golba, M. Sensitivity of Solar Photovoltaic Panel Efficiency to Weather and Dust over West Africa: Comparative Experimental Study between Niamey (Niger) and Abidjan (Côte d'Ivoire). *Comput. Water Energy Environ. Eng.* **2016**, *5*, 123–147. [CrossRef]
25. Hou, X.; Wild, M.; Folini, D.; Kazadzis, S.; Wohland, J. Climate Change Impacts on Solar Power Generation and Its Spatial Variability in Europe Based on CMIP6. *Earth Syst. Dyn.* **2021**, *12*, 1099–1113. [CrossRef]
26. Müller, J.; Folini, D.; Wild, M.; Pfenninger, S. CMIP-5 Models Project Photovoltaics Are a No-Regrets Investment in Europe Irrespective of Climate Change. *Energy* **2019**, *171*, 135–148. [CrossRef]
27. Danso, D.K.; Anquetin, S.; Diedhiou, A.; Lavaysse, C.; Hingray, B.; Raynaud, D.; Kobea, A.T. A CMIP6 Assessment of the Potential Climate Change Impacts on Solar Photovoltaic Energy and Its Atmospheric Drivers in West Africa. *Environ. Res. Lett.* **2022**, *17*, 044016. [CrossRef]
28. Bichet, A.; Hingray, B.; Evin, G.; Diedhiou, A.; Kebe, C.M.F.; Anquetin, S. Potential Impact of Climate Change on Solar Resource in Africa for Photovoltaic Energy: Analyses from CORDEX-AFRICA Climate Experiments. *Environ. Res. Lett.* **2019**, *14*, 124039. [CrossRef]
29. Adar, M.; Babay, M.-A.; Boussif, M.; Khaouch, Z.; Abbassi, Z.; Najih, Y.; Mabrouki, M. *Optimization of Photovoltaic System Modelling: A Comparative Study and Experimental Validation Using Bond Graph Methodology and a Genetic Algorithm*; IOS Press: Amsterdam, The Netherlands, 2024.
30. Sawadogo, W.; Reboita, M.S.; Faye, A.; da Rocha, R.P.; Odoulami, R.C.; Olusegun, C.F.; Adeniyi, M.O.; Abiodun, B.J.; Sylla, M.B.; Diallo, I.; et al. Current and Future Potential of Solar and Wind Energy over Africa Using the RegCM4 CORDEX-CORE Ensemble. *Clim. Dyn.* **2020**, *57*, 1647–1672. [CrossRef]
31. Sawadogo, W.; Abiodun, B.J.; Okogbue, E.C. Impacts of Global Warming on Photovoltaic Power Generation over West Africa. *Renew. Energy* **2019**, *151*, 263–277. [CrossRef]
32. Soares, P.M.M.; Brito, M.C.; Careto, J.A.M. Persistence of the High Solar Potential in Africa in a Changing Climate. *Environ. Res. Lett.* **2019**, *14*, 124036. [CrossRef]
33. Ndiaye, A.; Moussa, M.S.; Dione, C.; Sawadogo, W.; Bliefernicht, J.; Dungall, L.; Kunstmann, H. Projected Changes in Solar PV and Wind Energy Potential over West Africa: An Analysis of CORDEX-CORE Simulations. *Energies* **2022**, *15*, 9602. [CrossRef]
34. Knippertz, P.; Todd, M.C. Mineral Dust Aerosols over the Sahara: Meteorological Controls on Emission and Transport and Implications for Modeling. *Rev. Geophys.* **2012**, *50*, RG1007. [CrossRef]
35. Gbobaniyi, E.; Sarr, A.; Sylla, M.B.; Diallo, I.; Lennard, C.; Dosio, A.; Dhiédiou, A.; Kamga, A.; Klutse, N.A.B.; Hewitson, B.; et al. Climatology, Annual Cycle and Interannual Variability of Precipitation and Temperature in CORDEX Simulations over West Africa. *Int. J. Climatol.* **2014**, *34*, 2241–2257. [CrossRef]
36. Danso, D.K.; Anquetin, S.; Diedhiou, A.; Lavaysse, C.; Kobea, A.; Touré, N.E. Spatio-Temporal Variability of Cloud Cover Types in West Africa with Satellite-Based and Reanalysis Data. *Q. J. R. Meteorol. Soc.* **2019**, *145*, 3715–3731. [CrossRef]
37. N'Datchoh, E.T.; Kouadio, K.; Silué, S.; Bamba, A.; Naabil, E.; Djè, K.B.; Diedhiou, A.; Sylla, M.B.; Anquetin, S.; Lennard, C. Potential Changes in Temperature Extreme Events under Global Warming at 1.5 °C and 2 °C over Côte d'Ivoire*. *Environ. Res. Clim.* **2022**, *1*, 015007. [CrossRef]

38. Kouadio, K.; Konare, A.; Diawara, A.; Dje, B.K.; Ajayi, V.O.; Diedhiou, A. Assessment of Regional Climate Models over Côte D'Ivoire and Analysis of Future Projections over West Africa. *Atmos. Clim. Sci.* **2015**, *5*, 63–81. [CrossRef]
39. Kouadio, Y.; Aman, A.; Ochou, A.; Ali, K.; Assamoi, P. Rainfall Variability Patterns in West Africa: Case of Cote d'Ivoire and Ghana. *J. Environ. Sci. Eng.* **2011**, *5*, 1229–1238.
40. Giorgi, F.; Jones, C.; Asrar, G.R. Addressing Climate Information Needs at the Regional Level: The CORDEX Framework. *World Meteorol. Organ. WMO Bull.* **2009**, *58*, 175.
41. Giorgi, F.; Coppola, E.; Jacob, D.; Teichmann, C.; Abba Omar, S.; Ashfaq, M.; Ban, N.; Buelow, K.; Bukovsky, M.; Buntemeyer, L.; et al. The CORDEX-CORE EXP-I Initiative: Description and Highlight Results from the Initial Analysis. *Bull. Am. Meteorol. Soc.* **2022**, *103*, E293–E310. [CrossRef]
42. Teichmann, C.; Jacob, D.; Remedio, A.R.; Remke, T.; Buntemeyer, L.; Hoffmann, P.; Kriegsmann, A.; Lierhammer, L.; Bülow, K.; Weber, T.; et al. Assessing Mean Climate Change Signals in the Global CORDEX-CORE Ensemble. *Clim. Dyn.* **2021**, *57*, 1269–1292. [CrossRef]
43. Ndiaye, A.; Wane, D.; Dione, C.; Gaye, A.T. Assessing Solar Energy Production in Senegal under Future Climate Scenarios Using Regional Climate Models. *Sol. Energy Adv.* **2025**, *5*, 100101. [CrossRef]
44. Jacob, D.; Podzun, R. Sensitivity Studies with the Regional Climate Model REMO. *Meteorol. Atmos. Phys.* **1997**, *63*, 119–129. [CrossRef]
45. Giorgi, F.; Coppola, E.; Solmon, F.; Mariotti, L.; Sylla, M.B.; Bi, X.; Elguindi, N.; Diro, G.T.; Nair, V.; Giuliani, G.; et al. RegCM4: Model Description and Preliminary Tests over Multiple CORDEX Domains. *Clim. Res.* **2012**, *52*, 7–29. [CrossRef]
46. Rockel, B.; Will, A.; Hense, A. The Regional Climate Model COSMO-CLM (CCLM). *Meteorol. Z.* **2008**, *17*, 347–348. [CrossRef]
47. Jones, C.D.; Hughes, J.K.; Bellouin, N.; Hardiman, S.C.; Jones, G.S.; Knight, J.; Liddicoat, S.; O'Connor, F.M.; Andres, R.J.; Bell, C.; et al. The HadGEM2-ES Implementation of CMIP5 Centennial Simulations. *Geosci. Model Dev.* **2011**, *4*, 543–570. [CrossRef]
48. Giorgetta, M.A.; Jungclaus, J.; Reick, C.H.; Legutke, S.; Bader, J.; Böttinger, M.; Brovkin, V.; Crueger, T.; Esch, M.; Fieg, K.; et al. Climate and Carbon Cycle Changes from 1850 to 2100 in MPI-ESM Simulations for the Coupled Model Intercomparison Project Phase 5. *J. Adv. Model. Earth Syst.* **2013**, *5*, 572–597. [CrossRef]
49. Bentsen, M.; Bethke, I.; Debernard, J.B.; Iversen, T.; Kirkevåg, A.; Seland, Ø.; Drange, H.; Roelandt, C.; Seierstad, I.A.; Hoose, C.; et al. The Norwegian Earth System Model, NorESM1-M–Part 1: Description and Basic Evaluation of the Physical Climate. *Geosci. Model Dev.* **2013**, *6*, 687–720. [CrossRef]
50. Taylor, K.E.; Stouffer, R.J.; Meehl, G.A. An Overview of CMIP5 and the Experiment Design. *Bull. Am. Meteorol. Soc.* **2012**, *93*, 485–498. [CrossRef]
51. Pal, J.S.; Small, E.E.; Eltahir, E.A.B. Simulation of Regional-Scale Water and Energy Budgets: Representation of Subgrid Cloud and Precipitation Processes within RegCM. *J. Geophys. Res. Atmos.* **2000**, *105*, 29579–29594. [CrossRef]
52. Solmon, F.; Giorgi, F.; Liousse, C. Aerosol Modelling for Regional Climate Studies: Application to Anthropogenic Particles and Evaluation over a European/African Domain. *Tellus B Chem. Phys. Meteorol.* **2022**, *58*, 51–72. [CrossRef]
53. Zakey, A.S.; Solmon, F.; Giorgi, F. Implementation and Testing of a Desert Dust Module in a Regional Climate Model. *Atmos. Chem. Phys.* **2006**, *6*, 4687–4704. [CrossRef]
54. Zakey, A.S.; Giorgi, F.; Bi, X. Modeling of Sea Salt in a Regional Climate Model: Fluxes and Radiative Forcing. *J. Geophys. Res. Atmos.* **2008**, *113*, 2007JD009209. [CrossRef]
55. Doms, G.; Förstner, J.; Heise, E.; Herzog, H.J.; Raschendorfer, M.; Schrodin, R.; Reinhardt, T.; Vogel, G. A Description of the Nonhydrostatic Regional Model LM. Part II: Physical Parametrization. *Dtsch. Wetterd. Offenb.* **2005**. Available online: https://www.cosmo-model.org/content/model/cosmo/coreDocumentation/cosmo_physics_4.20.pdf (accessed on 12 April 2025).
56. Lohmann, U.; Roeckner, E. Design and Performance of a New Cloud Microphysics Scheme Developed for the ECHAM General Circulation Model. *Clim. Dyn.* **1996**, *12*, 557–572. [CrossRef]
57. Tanré, D.; Geleyn, J.F.; Slingo, J.M. First Results of the Introduction of an Advanced Aerosol-Radiation Interaction in the ECMWF Low Resolution Global Model. *Aerosols Their Clim. Eff.* **1984**, *133*, 177.
58. Hans Hersbach, W.B. Global Reanalysis: Goodbye ERA-Interim, Hello ERA5. Available online: https://www.ecmwf.int/en/elibrary/81046-global-reanalysis-goodbye-era-interim-hello-era5 (accessed on 4 December 2025).
59. Hersbach, H.; Bell, B.; Berrisford, P.; Hirahara, S.; Horányi, A.; Muñoz-Sabater, J.; Nicolas, J.; Peubey, C.; Radu, R.; Schepers, D.; et al. The ERA5 Global Reanalysis. *Q. J. R. Meteorol. Soc.* **2020**, *146*, 1999–2049. [CrossRef]
60. Gutowski, W.J., Jr.; Giorgi, F.; Timbal, B.; Frigon, A.; Jacob, D.; Kang, H.-S.; Raghavan, K.; Lee, B.; Lennard, C.; Nikulin, G.; et al. WCRP COordinated Regional Downscaling EXperiment (CORDEX): A Diagnostic MIP for CMIP6. *Geosci. Model Dev.* **2016**, *9*, 4087–4095. [CrossRef]
61. Wu, G.; Qin, S.; Mao, Y.; Ma, Z.; Shi, C. Validation of Precipitation Events in ERA5 to Gauge Observations during Warm Seasons over Eastern China. *J. Hydrometeorol.* **2022**, *23*, 807–822. [CrossRef]

62. Amega, K.; Laré, Y.; Bhandari, R.; Moumouni, Y.; Egbendewe, A.; Sawadogo, W.; Madougou, S. Solar Energy Powered Decentralized Smart-Grid for Sustainable Energy Supply in Low-Income Countries: Analysis Considering Climate Change Influences in Togo. *Energies* **2022**, *15*, 9532. [CrossRef]
63. Pfeifroth, U.; Kothe, S.; Müller, R.; Trentmann, J.; Hollmann, R.; Fuchs, P.; Werscheck, M. *Release of CM SAF Surface Radiation Data Set-Heliosat (SARAH)–Edition 2.1*; CMSAF: Arlington, VA, USA, 2017.
64. Pfeifroth, U.; Sanchez-Lorenzo, A.; Manara, V.; Trentmann, J.; Hollmann, R. Trends and Variability of Surface Solar Radiation in Europe Based on Surface-and Satellite-Based Data Records. *J. Geophys. Res. Atmos.* **2018**, *123*, 1735–1754. [CrossRef]
65. Ajayi, V.O.; Ilori, O.W. Projected Drought Events over West Africa Using RCA4 Regional Climate Model. *Earth Syst. Environ.* **2020**, *4*, 329–348. [CrossRef]
66. Akinsanola, A.A.; Ogunjobi, K.O.; Gbode, I.E.; Ajayi, V.O. Assessing the Capabilities of Three Regional Climate Models over CORDEX Africa in Simulating West African Summer Monsoon Precipitation. *Adv. Meteorol.* **2015**, *2015*, 935431. [CrossRef]
67. Zhang, J.; You, Q.; Ullah, S. Changes in Photovoltaic Potential over China in a Warmer Future. *Environ. Res. Lett.* **2022**, *17*, 114032. [CrossRef]
68. Schulzweida, U. *CDO User Guide*, version 2.3.0; Zenodo: Geneva, Switzerland, 2023. [CrossRef]
69. Mathewos, Y.; Abate, B.; Dadi, M. Characterization of the Skill of the CORDEX-Africa Regional Climate Models to Simulate Regional Climate Setting in the East African Transboundary Omo Gibe River Basin, Ethiopia. *Heliyon* **2023**, *9*, e20379. [CrossRef]
70. Kassahun, M.; Ture, K.; Nedaw, D. Correction: Evaluation of CORDEX Africa Regional Climate Models Performance in Simulating Climatology of Zarima Sub-Basin Northwestern Ethiopia. *Environ. Syst. Res.* **2023**, *14*, 5. [CrossRef]
71. Jerez, S.; Tobin, I.; Vautard, R.; Montávez, J.P.; López-Romero, J.M.; Thais, F.; Bartok, B.; Christensen, O.B.; Colette, A.; Déqué, M.; et al. The Impact of Climate Change on Photovoltaic Power Generation in Europe. *Nat. Commun.* **2015**, *6*, 10014. [CrossRef] [PubMed]
72. Mavromatakis, F.; Makrides, G.; Georghiou, G.; Pothrakis, A.; Franghiadakis, Y.; Drakakis, E.; Koudoumas, E. Modeling the Photovoltaic Potential of a Site. *Renew. Energy* **2010**, *35*, 1387–1390. [CrossRef]
73. TamizhMani, G.; Ji, L.; Tang, Y.; Petacci, L.; Osterwald, C. Photovoltaic Module Thermal/Wind Performance: Long-Term Monitoring and Model Development for Energy Rating. In Proceedings of the NCPV and Solar Program Review Meeting 2003, Lakewood, CO, USA, 24–26 March 2003.
74. Lasnier, F.; Ang, T.G. *Photovoltaic Engineering Handbook*, 3rd ed.; References-Scientific Research Publishing; CRC Press: Boca Raton, FL, USA, 1990. Available online: https://www.scirp.org/reference/referencespapers?referenceid=1910459 (accessed on 5 December 2025).
75. Crook, J.A.; Jones, L.A.; Forster, P.M.; Crook, R. Climate Change Impacts on Future Photovoltaic and Concentrated Solar Power Energy Output. *Energy Environ. Sci.* **2011**, *4*, 3101–3109. [CrossRef]
76. Ayugi, B.; Tan, G.; Gnitou, G.T.; Ojara, M.; Ongoma, V. Historical Evaluations and Simulations of Precipitation over East Africa from Rossby Centre Regional Climate Model. *Atmos. Res.* **2020**, *232*, 104705. [CrossRef]
77. Mendez, M.; Maathuis, B.; Hein-Griggs, D.; Alvarado-Gamboa, L.-F. Performance Evaluation of Bias Correction Methods for Climate Change Monthly Precipitation Projections over Costa Rica. *Water* **2020**, *12*, 482. [CrossRef]
78. Schober, P.; Boer, C.; Schwarte, L.A. Correlation Coefficients: Appropriate Use and Interpretation. *Anesth. Analg.* **2018**, *126*, 1763. [CrossRef]
79. Yersaw, B.T.; Chane, M.B.; Yitayew, N.A. Performance Evaluation of Varies Climate Models Using Observed and Regional Climate Models for the Katar Watershed, Ethiopia. *Environ. Syst. Res.* **2024**, *13*, 14. [CrossRef]
80. Evans, J.D. *Straightforward Statistics for the Behavioral Sciences*; Thomson Brooks/Cole Publishing Co.: Belmont, CA, USA, 1996; pp. xxii, 600, ISBN 978-0-534-23100-2.
81. Geleta, C.D.; Gobosho, L. Climate Change Induced Temperature Prediction and Bias Correction in Finchaa Watershed. *Environ. Sci.* **2018**, *18*, 324–337.
82. Chai, T.; Draxler, R.R. Root Mean Square Error (RMSE) or Mean Absolute Error (MAE)?—Arguments against avoiding RMSE in the literature. *Geosci. Model Dev.* **2014**, *7*, 1247–1250. [CrossRef]
83. Wilcox, L.J.; Highwood, E.J.; Booth, B.B.B.; Carslaw, K.S. Quantifying Sources of Inter-Model Diversity in the Cloud Albedo Effect. *Geophys. Res. Lett.* **2015**, *42*, 1568–1575. [CrossRef]
84. Boucher, O.; Randall, D.; Artaxo, P.; Bretherton, C.; Feingold, G.; Forster, P.; Kerminen, V.-M.; Kondo, Y.; Liao, H.; Lohmann, U.; et al. Clouds and Aerosols. In *Climate Change 2013–The Physical Science Basis: Working Group I Contribution to the Fifth Assessment Report of the Intergovernmental Panel on Climate Change*; Intergovernmental Panel on Climate Change (IPCC), Ed.; Cambridge University Press: Cambridge, UK, 2014; pp. 571–658, ISBN 978-1-107-05799-9.
85. Wilcox, L.J.; Highwood, E.J.; Dunstone, N.J. The Influence of Anthropogenic Aerosol on Multi-Decadal Variations of Historical Global Climate. *Environ. Res. Lett.* **2013**, *8*, 024033. [CrossRef]
86. Tang, C.; Morel, B.; Wild, M.; Pohl, B.; Abiodun, B.; Bessafi, M. Numerical Simulation of Surface Solar Radiation over Southern Africa. Part 1: Evaluation of Regional and Global Climate Models. *Clim. Dyn.* **2019**, *52*, 457–477. [CrossRef]

87. Palmer, T.N. A Personal Perspective on Modelling the Climate System. *Proc. Math. Phys. Eng. Sci.* **2016**, *472*, 20150772. [CrossRef] [PubMed]
88. Solomon, S.; Plattner, G.-K.; Knutti, R.; Friedlingstein, P. Irreversible Climate Change Due to Carbon Dioxide Emissions. *Proc. Natl. Acad. Sci. USA* **2009**, *106*, 1704–1709. [CrossRef] [PubMed]